Journal of Crystal Growth 603 (2023) 126986

Contents lists available at ScienceDirect

Journal of Crystal Growth

journal homepage: www.elsevier.com/locate/jcrysgro

Understanding the agglomerate crystallisation of hexamine through X-ray microscopy and crystallographic modelling

Thai T.H. Nguyen [a,*], Parmesh Gajjar [b,e,1], Jun Sun [c], Robert B. Hammond [a], Darragh Murnane [d], Benjamin Tordoff [f], Erik Lauridsen [c], Philip J. Withers [b,e], Kevin J. Roberts [a,*]

[a] Centre for the Digital Design of Drug Products, School of Chemical and Process Engineering, University of Leeds, Leeds, UK
[b] Henry Moseley X-ray Imaging Facility, Department of Materials, The University of Manchester, Manchester M13 9PL, UK
[c] Xnovo Technology ApS, Galoche Alle 15, 1, 4600 Koege, Denmark
[d] School of Life and Medical Sciences, University of Hertfordshire, College Lane, Hatfield AL10 9AB, UK
[e] Henry Royce Institute for Advanced Materials, Department of Materials, University of Manchester, Manchester M13 9PL, UK
[f] Carl Zeiss Microscopy GmbH, Carl-Zeiss-Straße 22, 73447 Oberkochen, Germany

ARTICLE INFO

Communicated by James J. De Yoreo

Keywords:
A1. Morphological stability
A1. Supersaturated solutions
A1. X-Ray computed tomography
A1. Computer simulation
A2. Growth from solutions

ABSTRACT

The detailed molecular-scale mechanism of the growth of organic crystals underpins a diversity of phenomena, such as the isolation and purification of high-quality materials for the pharmaceutical and fine chemical sectors. Recent advances in X-ray Microscopy (XRM) and complementary diffraction contrast tomography (DCT) have enabled the detailed characterisation of the micro-structure of hexamine agglomerates. Detailed XRM analysis of the growth history and micro-structure of such agglomerates reveals a highly orientated epitaxial inter-relationship between their constituent micro-crystallites. This is found to be consistent with a secondary nucleation growth mechanism associated with re-growth at the 3-fold corner sites within the crystals' dominant {1 1 0} dodecahedral morphology. The agglomeration appears to heal upon further growth as the aligned agglomerated micro-crystals connect and fuse together but, in doing so, pockets of inter-crystallite mother liquor become trapped forming a symmetric pattern of solvent inclusions. The mechanistic origin of this phenomenon is rationalised with respect to historical data together with an analysis of the solid-state chemistry of the compound through the development of a 'snow flake' model. The latter draws upon hexamine's propensity for edge growth instabilities with increasing crystal size as well as its tendency for unstable growth at the facet corners along the ⟨1 1 1⟩ directions, a situation compounded by the lack of growth-promoting dislocations at the centers of the {1 1 0} habit surfaces. The agglomerative mechanism presented here could apply to other high symmetry crystal systems, particularly those whose crystal structures involve centred Bravais lattices and where the dominant inter-molecular interactions are angled towards the facet edges.

1. Introduction

Hexamine, which was first prepared in 1859 [1], is a condensation product formed readily from gaseous, aqueous, or organic solutions of ammonia and formaldehyde. Hexamine is a significant molecule historically, as it was the first organic crystal to have its structure determined by X-ray diffraction and spectrometric measurements almost 100 years ago [2–4]. Hexamine is a highly symmetric molecule, which crystallises in a body-centred cubic crystal structure giving rise to a highly equant dodecahedral crystal morphology. It has been widely used as an intermediate chemical, mainly used in organic synthesis [5], in coordination polymer production, and for applications within the resin industry. Hexamine crystals can be easily recrystallized from aqueous and ethanolic solutions as they are quite soluble in water,but in common with some other tertiary amines, their solubility in water decreases with increasing temperature [6]. Methods have been developed for growing large crystals of hexamine from aqueous or alcoholic solutions [7,8], as well as from the vapour phase [9]. The growth kinetics for hexamine crystallization from aqueous solution and pure ethanol have also been determined [10–12].

Hexamine is also of fundamental significance as a crystalline compound in terms of its crystal chemistry and habit. Previous characterisation studies on hexamine have highlighted its interesting

* Corresponding authors at: School of Computing, University of Leeds, Woodhouse Lane, Leeds LS2 9JT, UK (T.H. Nguyen).
E-mail addresses: H.Nguyen1@leeds.ac.uk (T.T.H. Nguyen), K.J.Roberts@leeds.ac.uk (K.J. Roberts).
[1] Present address: Seda Pharmaceutical Development Services, Unit D Oakfield Road, Cheadle Royal Business Park, Cheadle SK8 3GX, UK.

https://doi.org/10.1016/j.jcrysgro.2022.126986
Received 4 July 2022; Received in revised form 1 November 2022; Accepted 9 November 2022
Available online 21 November 2022

Nomenclature

List of symbols and abbreviations

ΔH_{sub}	Experimental sublimation enthalpy
R	Molar gas constant
T	Temperature
E_{cr}	Lattice Energy
E_{slice}	Slice Energy
E_{att}^{hkl}	Attachment Energy
ξ_{hkl}	Anisotropy factor
d_{hkl}	Inter-planar spacings
$\underline{n}$	Growth direction
$\underline{b}$	Burgers vector
$\underline{l}$	Dislocation line direction
XRM	X-ray Microscopy
XCT	X-ray computed tomography
LabDCT	laboratory diffraction contrast tomography

crystallization properties, notably its propensity for inter-crystal agglomeration [13] and the trapping of solvent inclusions due to growth instabilities [14] as well as, at times, its high degree of crystallographic perfection [8], and its distinctive symmetrical patterns of solvent inclusions [15].

The growth morphology of crystalline materials has been of long-standing interest dating back to the work of Gibbs [16] and Wulff [17] on the equilibrium form of crystals. Interfacial stability [18] as well as the stability of the crystal growth process taking place on the facets of growing crystals [19] have also been important areas of research in understanding the morphology of crystals. Many organic materials find practical applications as polycrystalline solids, and hence an extensive evaluation of the physico-chemical and particle properties of these materials is important, notably through an evaluation of the inter-dependence between their structure, properties, processing and performance [20,21].

The presence of inclusions within the particles during crystallization can be problematic as these may occupy a significant fraction of the total crystal volume, which can manifest in the form of a considerable quantity of impurity in the final products [14]. Hexamine provides an excellent perspective on the importance of understanding, characterising and controlling the crystal morphology, growth stability and hence the powder behavior of crystalline powders [22] due to the potential impact of any variation in crystal microstructure and habit on the chemical and physical stabilities, and on downstream processing behavior [23]. For example, hexamine powders are hygroscopic, and extensive moisture-induced crystalline bridging has been observed in crystalline powders [24]. In this respect, molecular modelling of the intermolecular arrangements both within, and at, the surfaces of crystalline materials has proved to be a useful tool to aid the design of products and the processes used for their manufacture. By understanding the spatial arrangements of the constituent molecules and their intermolecular interactions (synthons) [25] within the crystallographic structures of a material, it is possible to predict and control the properties of the crystalline particles. Such synthonic engineering techniques have been used to predict the crystal morphology and particle properties [26–29], the mediation of crystal growth by solvent [30], additives or impurities [31–33], and the physical and chemical properties of the formulated compounds [34,35]. These approaches have also used, for example, in the design of crystallisation processes as well as their subsequent formulation into desired products [35,36].

Recent work [24] has also highlighted the utility of X-ray computed tomography (XCT) and laboratory X-ray diffraction contrast tomography (LabDCT) in the characterisation of the interfacial properties of agglomerated powders and agglomerated crystals of hexamine, notably the granular structure of powders, as well as their preferred orientation both within the powder bed and within the individual agglomerated particles. In this paper, we have examined such behaviour in more detail by combining XCT and LabDCT data with molecular- and intermolecular modelling to provide a detailed analysis of the crystal morphology, morphological instability and assessment of the micro-structures of particle agglomerates. The work seeks to probe the fundamental molecular-scale processes associated with the agglomerative crystallisation of hexamine and how such behaviour might be potentially controlled to improve crystal quality.

2. Material and methods

2.1. Materials

Hexamine, chemical formula $(CH_2)_6N_4$, crystallises in the highly symmetrical but non-centrosymmetric cubic space group $I-43m$ with two molecules in a body-centred unit cell (see Fig. 1) with a lattice parameter of 6.927 Å [37]. The molecular structure is slightly polar in nature with dipoles along the ⟨1 1 1⟩ directions.

For the experimental work, hexamine (≥98 %) and ethanol (anhydrous) was purchased from Sigma-Aldrich.

2.2. Experimental methods

For the preparation of hexamine crystals, a suspension containing 0.0486 g/g of hexamine in ethanol, prepared in a 100 mL HEL AutoMATE glass multi-crystalliser system (https://helgroup.com/), was constantly stirred at a rate of ~500 rpm. The solution was heated from room temperature to 50 °C at a heating rate of 1 °C/min and held at 50 °C for 15 min to ensure complete dissolution. The solution was then cooled to 5 °C at a slow cooling rate of 0.1 °C/min and kept constant at 5 °C. Around one day after nucleation, the product crystals were isolated from the solutions using a VacMaster 10 vacuum pump system and the filtered samples were dried at room temperature under a fume hood.

2.3. X-ray microscopy (XRM) and diffraction contrast tomography

A 3 mm diameter Kapton tube was filled with hexamine crystals and mounted on a Zeiss Xradia Versa 520 XRM instrument fitted with a LabDCT module [38]. An attenuation X-ray CT scan was performed at the top of the powder bed, followed by 3 overlapping diffraction datasets for LabDCT characterization. The attenuation X-ray CT scan was reconstructed using the Zeiss XMReconstructor software provided on the XRM instrument (Carl Zeiss Microscopy, USA), which is based upon the FDK algorithm for cone-beam tomography acquisition [39]. The LabDCT data was reconstructed using the GrainMapper3D (Xnovo Technology ApS) version 2.2 software. Full details of the scanning and reconstruction parameters are available elsewhere [24].

Image analysis was performed on the reconstructed tomographic data using a combination of Dream3D (BlueQuartz Software, USA) and Dragonfly Pro version 4.1 (Object Research Systems, Canada) with the individual agglomerates being separated using the separate objects function in Dragonfly Pro. In order to characterise the internal microstructure of the agglomerates, the images of the individual crystallites were aligned normal to ⟨1 1 1⟩ crystallographic directions. This was accomplished by an iterative procedure, with the plane orientation adjusted until the internal angles of a cross-sectional slice taken at a 3-fold corner site were all close to 60°, with the projection in this orientation consistent with the 3-fold symmetry around the ⟨1 1 1⟩ direction as shown in Fig. 2. Following this, a series of cross-sectioned images, parallel to this plane, were taken from a number of crystals displaying varying external perfection.

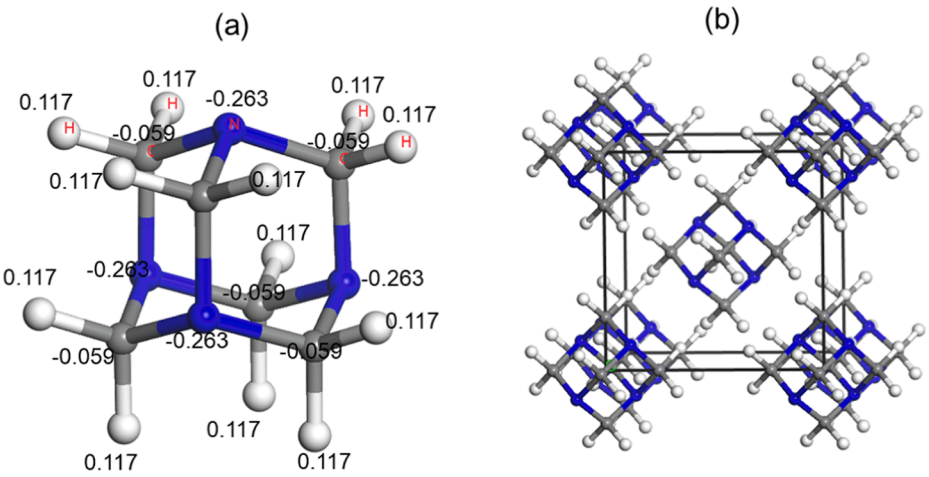

Fig. 1. Molecular and intermolecular structure for hexamine showing (a) the molecular structure with the atomic fractional charges and (b) the projection of the unit cell down the c-axis showing the intermolecular packing for the body-centered cubic crystal system.

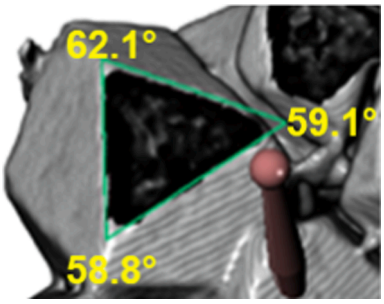

Fig. 2. A 3D rendering from XCT data, showing how to slice agglomerates by aligning the particle along a ⟨1 1 1⟩ direction close to the 3- fold corner site. The plane orientation was adjusted until the angles were all close to 60°.

2.4. Computational modelling

The intermolecular interaction energies and lattice energy (E_{cr}) for hexamine were calculated by the atom–atom method [40] using the Dreiding [41] empirical force field using HABIT98 [27,42] and validated with respect to the experimental sublimation enthalpy (ΔH_{sub}), thus:

$$E_{cr} = \Delta H_{sub} - 2RT \quad (1)$$

where R is the molar gas constant and T is temperature.

The likely morphologically-important crystal faces (*hkl*) were determined using the BFDH method [43–45] and the inter-molecular interactions were partitioned between those satisfied at the surface (E_{slice}) and those terminated at the growth surface (E_{att}) where.

$$E_{cr} = E_{att}^{hkl} + E_{slice}^{hkl} \quad (2)$$

The crystal morphology was predicted using the attachment energy method [46] and visualized using a Wulff plot [17] based upon the relative growth rates for the crystal habit surfaces R^{hkl}, thus:

$$R^{hkl} \sim E_{att}^{hkl} \quad (3)$$

The anisotropy factor is a helpful measure of crystal surface stability, i.e. it reflects the % of the intermolecular interactions that are satisfied at the crystal surface. Hence, the most stable slow growing crystal faces would have the smallest attachment energies or the largest anisotropy factor, ξ_{hkl}. The latter can be given by:

$$\xi_{hkl} = \frac{E_{slice}}{E_{cr}} \quad (4)$$

3. Results

3.1. Crystal chemistry and morphological characterisation

Crystallographic modelling of the hexamine crystal structure reveals two main intermolecular synthons: synthon A, along the ⟨1 1 1⟩ directions (i.e. between the corner and body-centred cubic molecules) with a strength of −1.56 kcal/mol and synthon B, along the ⟨1 0 0⟩ directions with a strength of −0.61 kcal/mol (see Fig. 3).

The predicted morphology for hexamine is summarised in Fig. 4. It shows good agreement with the observed crystals grown from both solution [7] and vapour [9] phases. The dodecahedral crystal habit of hexamine is characterized by the {1 1 0} form whose intersections represent two types of corners sites: six of which (labelled B) are termini of the four-fold inversion axes along the ⟨1 0 0⟩ directions, and eight of which (labelled A) are termini of the three-fold rotation axes along the ⟨1 1 1⟩ directions. A detailed analysis of intermolecular packing, crystal chemistry and calculated surface attachment energies for the morphologically important forms of hexamine are provided in the supplementary data (Section S1).

3.2. X-Ray computed tomography characterization of agglomerate structure

Fig. 5 shows the results obtained from four selected representative agglomerates, labelled B, E, F, and H that display different external morphologies and internal perfections (previously identified in [24]), which have been examined in more detail by characterising their internal micro-structure and, potentially, their mechanism of formation. The current particle labeling maintains consistency with the previous work [24] for ease of cross-comparison. Of those examined in detail using XCT and in most cases DCT, particle E exhibited the highest degree of crystal perfection, followed by particle H which consisted of an intergrowth between several domains, albeit one that was encompassed within a well-defined external particle morphology. Examination of particle B revealed it to comprise a well-defined agglomerate of at least 8 constituent microcrystals. Finally, and in contrast to particles E, H and B, particle F was observed to display a rather poorly-formed and rough external particle morphology, and one that was found to contain many internal solvent inclusions.

3.2.1. Particle E

Both the DCT data in Fig. 5(b) and XRM data in Fig. 6(a) reveal particle E to have a high crystallographic perfection with a well-defined

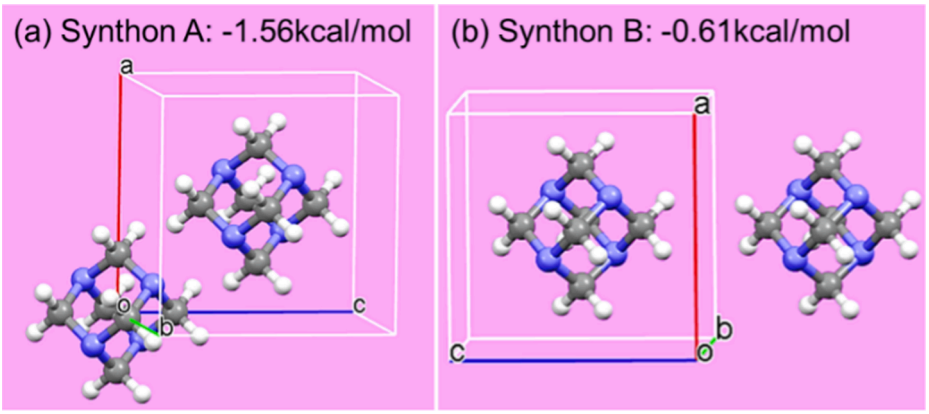

Fig. 3. The two strongest intermolecular interactions in crystal lattice of hexamine: synthon A and synthon B, adapted after [24].

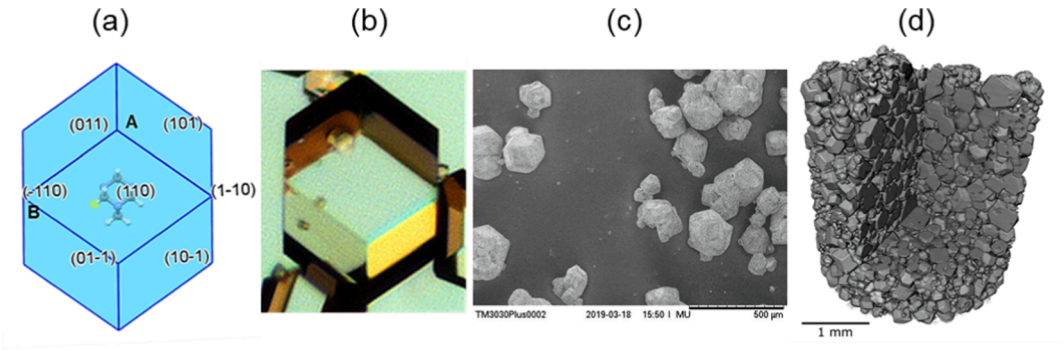

Fig. 4. Morphological data for hexamine: (a) The predicted morphology of hexamine viewed looking down [1 1 0] showing a rhombic dodecahedron with the 12 faces of {1 1 0} family. The three-corner in the ⟨1 1 1⟩ direction is labelled (A) and the four-corner in the [1 0 0] direction is labelled (B); (b) Optical microscopy image showing the rhombic dodecahedron crystal morphology; (c) SEM image of typical hexamine crystals; (d) Virtual volume representation of a hexamine powder bed from XCT, showing the crystal morphology throughout the powder bed. This figure reproduced in part after [24] and provided courtesy of the Royal Society of Chemistry.

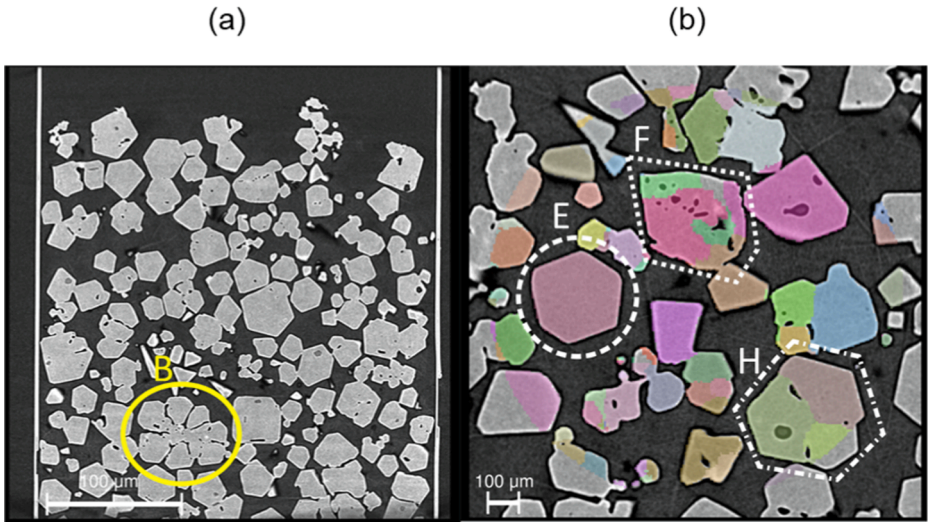

Fig. 5. (a) XCT data of powder bed showing a virtual cross-sectional slice in the vertical direction; (b) DCT data showing the indexing of individual crystallites through DCT, assigning a different (random) colour to each indexed crystallite. Data taken from our reference [24] published in CrystEngComm. Data reproduced after [24] courtesy of RSC.

external crystal morphology apparently revealing the particle to comprise a single domain. Examination of the 2D cross-sectioned slices confirms this orientation close to the {1 1 1} lattice planes (Fig. 6(b)). The 2D cross-sectional slices from the XRM data shown in (Fig. 6(c)-(f)) are indicative of the crystal's growth history which reveal evidence for the secondary nucleation of crystallites at the corner sites (labelled A) followed by solution trapping (Fig. 6(d)) and the subsequent overgrowth and 'healing' of the trapped solvent pocket.

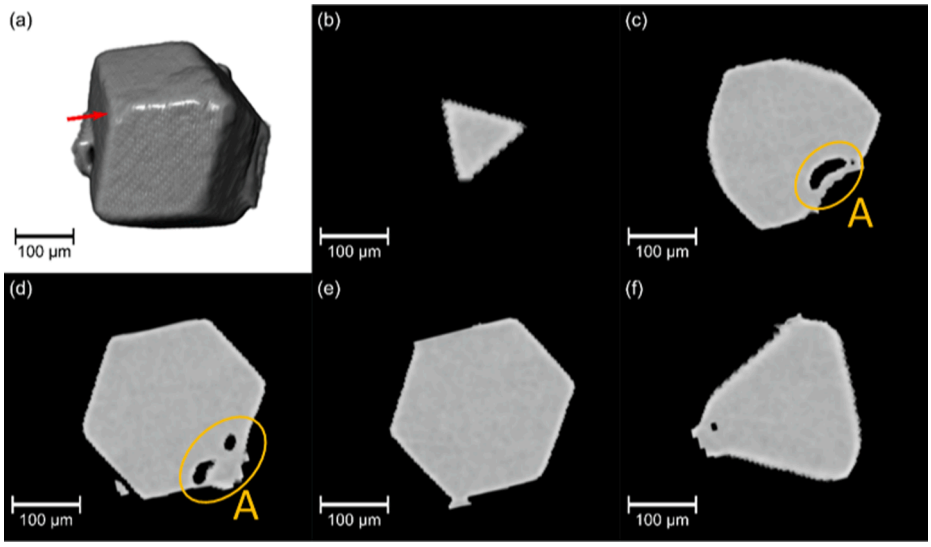

Fig. 6. XCT data for particle E: (a) A 3D visualisation of a single hexamine crystal; (b-f) A series of 2D cross sectional slices, 51 μm apart, taken in the ⟨1 1 1⟩ direction marked by the red arrow in (a). (For interpretation of the references to color in this figure legend, the reader is referred to the web version of this article.)

3.2.2. *Particle H*

Both the DCT data and 3D XRM data in Fig. 5 (b) and Fig. 7 (a) respectively, clearly reveal particle H to be an agglomerate of several crystals that have inter-grown. Nonetheless, both the internal and external perfection is clearly quite high with evidence from the diffraction data for lattice coherence between the sub-crystallites and a well-formed external morphology. This observation would be consistent with the 3 domains exhibiting a high degree of lattice coherence. The semi-transparent 3D visualisation (Fig. 7(b)) of the crystal reveals significant internal voiding that is also evident in the 2D cross-sectional slices from the XRM data. Fig. 7 (d-f) reveal solution-trapping (labelled B) at the re-entrant features (labelled C) consistent with secondary nucleation and re-growth.

3.2.3. *Particle F*

Both DCT and XRM data in Fig. 5(b) and Fig. 8(a), respectively, reveal the perfection of particle F to be quite poor both in terms of its internal perfection and its overall crystal morphology. The DCT data suggests it comprises three main domains with a micro-structure. The latter microstructure could potentially be consistent with unstable intergrowth behavior associated with the trapping of many solvent inclusions. The intergrowth behaviour has occurred in a manner suggesting its constituent crystals are very small and poorly-defined, such that this particle has resulted from the agglomeration from the large number of micro-crystals. This aspect is highlighted in the semi-transparent visualisation, Fig. 8(b), which reveals the particle to contain a substantial number of solution inclusions, as shown in Fig. 8 (f), and to exhibit a comparatively rough external morphology (Fig. 8(c-h)) which would be typical of unstable crystal growth. Examination of the DCT data (Fig. 5 (b)) reveals numerous domains within the particle but the lack of any defined faceted form would suggest that these domains probably themselves consist of a number of aligned micro-crystals.

3.2.4. *Particle B*

XRM analysis of the powder bed revealed the well-formed multi-crystal agglomerate particle B, shown in Fig. 5(a) for which the 3D imaging data is given in Fig. 9(a). The agglomerate displays high external perfection with well-formed facets on all its individual sub-crystallites. Analysis of the 2D cross-sectional slices from the XRM

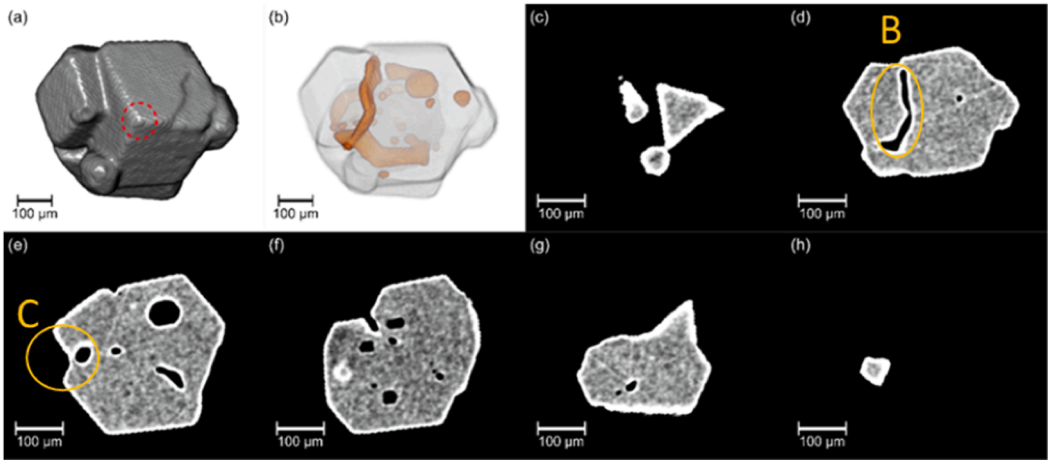

Fig. 7. XCT data for particle H:(a) A 3D visualisation of an agglomerate of hexamine crystals of high internal and external perfection; (b) A semi-transparent visualisation, with internal voids highlighted in orange; (c-h) A series of 2D slices, 37 μm apart, taken in the ⟨1 1 1⟩ direction. This direction is into the page in (a), with the 3-fold corner in the ⟨1 1 1⟩ direction marked by a red circle. (For interpretation of the references to color in this figure legend, the reader is referred to the web version of this article.)

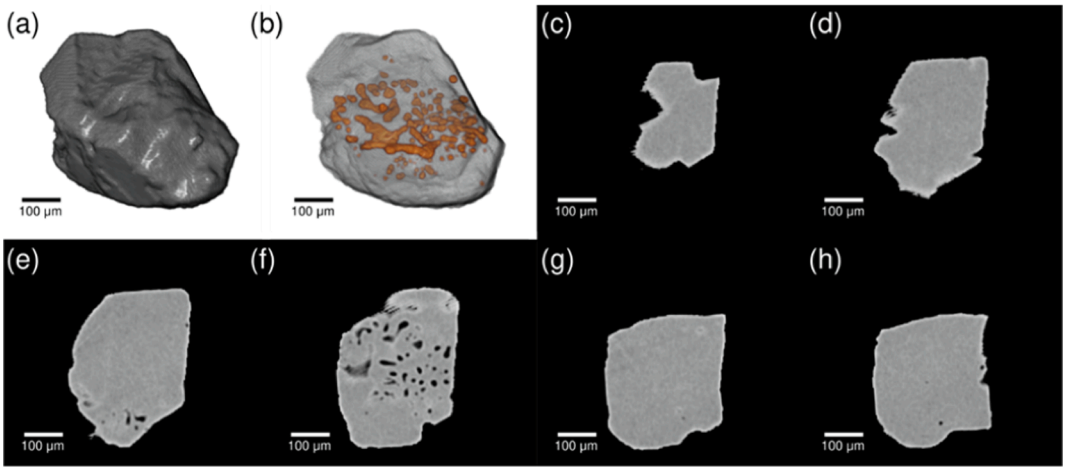

Fig. 8. XCT data for particle F(a) A 3D visualisation of a single hexamine crystal or agglomerate of poor internal perfection; (b) Semi-transparent visualisation with the internal voids highlighted in orange; (c-h) A series of 2D cross sectional slices, 51 μm apart, taken in the ⟨1 1 1⟩ direction. (For interpretation of the references to color in this figure legend, the reader is referred to the web version of this article.)

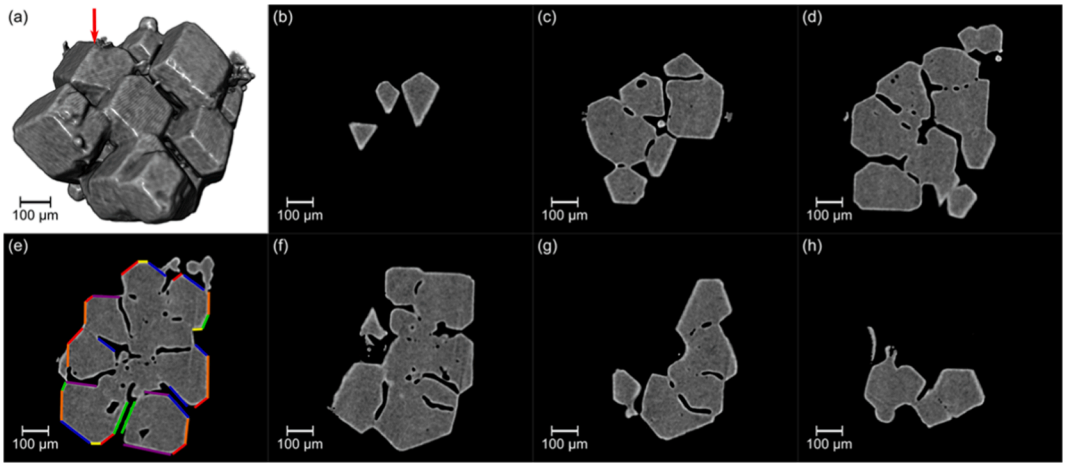

Fig. 9. XCT data for particle B for: (a) 3D rendering highlighting the numbers of agglomerated single particles and their mutual alignment showing a direction of a cut into agglomerate when aligned along the 3-fold crystal axis; (b) 2D slice of view highlighting identification of 3 fold axis using equilateral triangular alignment method; (c-h) successive set of 2D slices cut though agglomerate (separated by 37 μm) noting the epitaxial mutual alignments of the agglomerate's constituents crystals as highlighted in the colour coding (red, orange, yellow, blue and green) shown in (e). In this, each color refers a set of epitaxially aligned crystal faces in the different micro-crystals within the agglomerate.

data (Fig. 9 (b-h)) reveals very close alignment (highlighted by color coding) between all the crystallites consistent with an epitaxial crystal lattice alignment between its constituent crystallites.

4. Discussion

4.1. Comparison with previous crystallisation studies

The results of the X-ray computed tomography characterisation are broadly consistent with previous studies [14,15,47,48] which highlighted that hexamine crystals prepared by solvent evaporation and at the growth rates greater than 12 μm/minute tended to display patterns of solvent inclusions when the crystal size was greater than ca. 65 μm. These inclusions were found to encompass both a well-ordered and a random structure of inclusions with the former displaying the symmetrical alignment of 12 inclusions shown in Fig. 10 consistent with hexamine's dodecahedral crystal symmetry. The current work also highlighted the presence of what Denbigh and White [14] refered to as 'cavitites' which they defined as depressions at the facet centres, as well as noting a propensity for unstable growth step motion from the edges of the facets. A theoretical basic for such an edge nucleation growth instability as a function of crystal size, surface nucleation cluster size and growth rate had also been previously described [19], whilst a reduction of supersaturation and hence growth at the facet centres with increasing crystal size has also been previously highlighted [49–51].

The observation of solvent inclusions in the current study are also consistent with previous studies [14,15,47], confirming that hexamine crystals can display both ordered and random inclusion patterns. In this case, it appears that the inclusions could be random, but closer analysis of the patterns showed fascinating findings. It is interesting to note that whilst all the previous work on inclusions was performed on the analysis of projected images of the hexamine crystals, XRM now allows the possibility for a more complete 3D analysis, not only of the agglomerates, but also of their internal micro-structure. This reveals that the voids between the crystals become encapsulated by subsequent crystallisation, and also explains the overgrowths and the symmetrical inclusions [14,15,47]. Both overgrowths and symmetrical inclusions have been demonstrated in the previous literature [13], where many of the author's isolated crystals exhibited the same symmetrical pattern of inclusions (e.g. see Fig. 11). These have spatial positions corresponding to

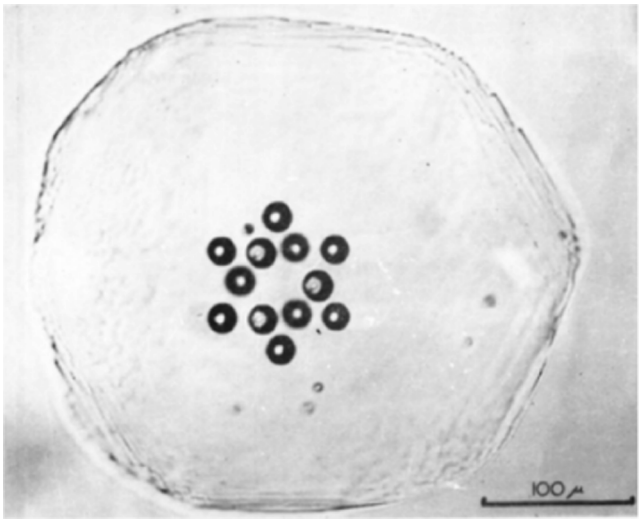

Fig. 10. Photograph of hexamine crystal showing arrangement of inclusions in crystal, after Denbigh and White [14], reproduced with permission Chemical Engineering Science.

the centres of the faces of a regular dodecahedron aligned with its faces parallel to the crystal. The regularity of their pattern suggested that their mechanism of formation might be closely linked to the crystal symmetry of hexamine and, in particular, to the direction of its strong intermolecular interactions. Examination of the growth history of the crystals would seem to suggest that these regular patterns of inclusions formed whilst the crystals were growing and that the re-entrant features observed within the external morphology are the direct result of the inter-crystal interactions leading to the formation of inclusions. This would suggest a facet corner-driven mechanism which leads eventually to the formation of overgrowths with further growth which, in doing so, trap pockets of solution. This is supported by previous data [13], reproduced in Fig. 13, which shows hexamine crystals after nucleation (a) and showing the intergrowth of the constituent crystals giving initially a rather imperfect form (b). After a further 5 mins of growth, the crystals display a regular hexagonal projected outline (c) with the re-entrant surface features being healed by overgrowth and solvent trapping. The void pockets of solution might be expected to continue to grow internally until the trapped solution is de-supersaturated. Further evidence for these phenomena have previously been provided [13] where hexamine was crystallised via acetone anti-solvent drown-out from aqueous solutions which highlighted the strong dependence of the crystal form on the solution supersaturation. The latter was observed to be well-formed single crystals at low supersaturations, which become agglomerated, and then dendritic with increasing supersaturation.

4.2. Agglomerate growth mechanisms

As previously identified [14,15,47], two distinct types of growth behavior can be identified: size-dependent surface instabilities and secondary nucleation at higher supersaturations at the facet corners leading to the formation of satellite crystals which subsequently coalesce overgrowth and heal.

4.2.1. Crystal size-dependent instability

In this mechanism, the hexamine crystal grows initially with well-defined stable growth with planar faces. But at a certain crystal size, solute mass transfer to the centres of the crystals reduces and hence the edges of the crystal begin to grow more rapidly resulting in cavity hollows (“cavitites”) at the centers of each face. As this preferential edge growth continues, the hollows in the faces form larger cavities which sink into the depths of the crystal creating solution inclusions [52]. At a later stage, the surfaces of the crystal may heal over, forming planar faces again and trapping solvent pockets within the crystals. When examined post-growth, these inclusions display a symmetrical pattern of inclusions having the shape of the original cavities with a spatial distribution consistent with the external dodecahedral morphology of the crystals [15]. Overall, from a mechanistic perspective, the formation of these inclusions can be associated with an unstable interfacial growth process due to a preference for facet edge-nucleation against the more stable step/terrace growth, reflecting reduced mass transfer to the surfaces as the crystal size increases. This effect is more pronounced at the higher supersaturations.

4.2.2. Instability due to secondary nucleation at facet corners

The growth instabilities can also lead to secondary nucleation at the facet corner sites leading to the formation of new crystals but ones, as confirmed by DCT, that are epitaxially aligned with respect to the ‘parent’ nucleating crystals. As shown schematically in Fig. 12, these new crystals will, through subsequent growth, form inter-crystal contacts trapping growth solution along their retreating edges. Initially, the leading edges of the secondary crystals form re-entrant features in the external morphology. In time, this heals over yielding a multi-crystal particle with an internal microstructure exhibiting strong epitaxial alignment and hence one that appears, and arguably is, a single crystal. Overall, from a mechanistic perspective, the formation of these inclusions can be associated with rapid and unstable crystal growth phenomenon which overall can be rationalized through a model whereby the fast-growing crystals produced at the higher supersaturations experience growth instability and form inclusions whilst the slow growing ones at the lower supersaturations do not.

4.3. The role played by growth-promoting dislocations

It is well-known that the presence of crystal lattice defects, such as screw dislocations, can play an important role in the generation of the surface step/terraces that are needed to facilitate stable crystal growth on facetted crystal surfaces [53]. Hexamine has a body-centred cubic crystal structure and so the Burgers vectors for the most likely low energy dislocations would be expected to be associated with the short intermolecular contact along the body diagonal of the unit cell i.e. ½

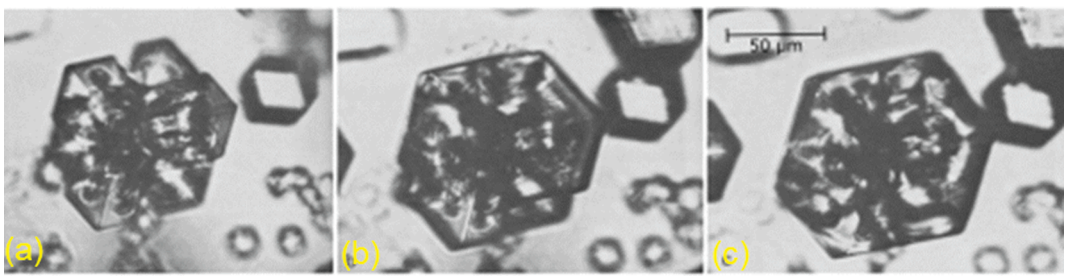

Fig. 11. Temporal sequence showing the crystal growth of hexamine in every 5mins, after Davey and Rutti [13], reproduced with permission from Journal of Crystal Growth.

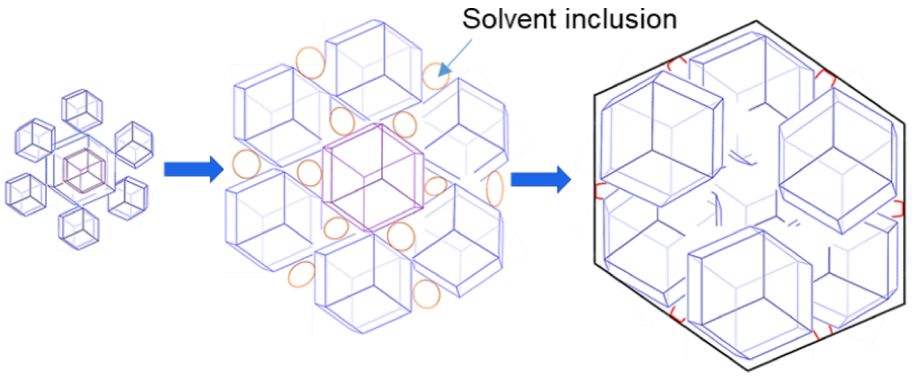

Fig. 12. Schematic showing a potential model for the secondary nucleation of hexamine along the ⟨1 1 1⟩ direction of synthon A, i.e. initial nucleation at the 3-fold corner sites followed by inter-crystal interaction and re-entrant formation which heal over with further growth.

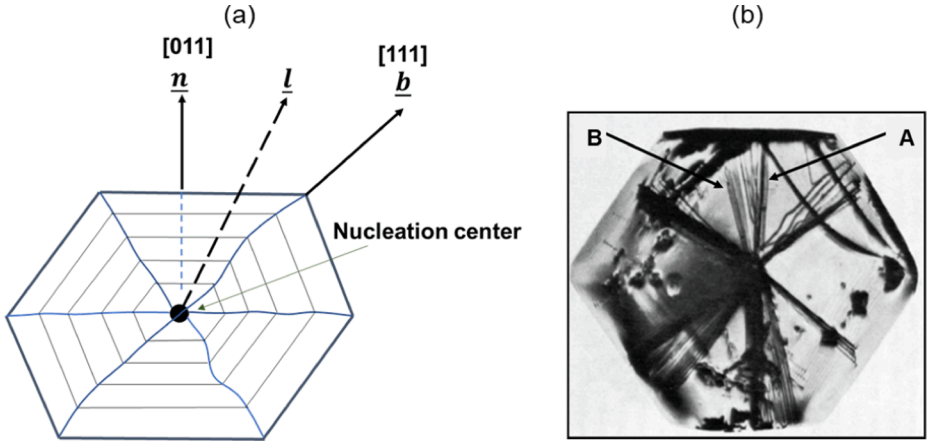

Fig. 13. (a) Schematic diagram showing the preferred dislocation trajectory associated with the growth direction, n, the dislocation line direction, l and the Burgers vector, b in hexamine crystals; (b) X-ray diffraction topography of a whole facetted crystal of hexamine, about 5 mm in size, as grown by solvent evaporation from ethanolic solution at ca. 21 °C highlighting the growth defect structure of a fairly typical solution grown organic crystal. Note the formation of two types of dislocations (dark lines, labelled A and B) emanating from the nucleation centre of the crystal which intersect the {1 1 0} habit surfaces of the crystal's dodecahedral morphology during the growth process (after Duckett and Lang 1973 and reproduced with permission by Elsevier, Journal of Crystal Growth).

⟨1 1 1⟩. For there to be a pure screw dislocation propagating normal to the {1 1 0} faces, the Burgers vector would need to be ⟨1 1 0⟩ which would have a high energy of formation and hence would be unlikely to form. The expected dislocation types for a body centred cubic lattice and a dodecahedral growth form have been previously analysed [54] based on the theory of preferred dislocations line directions developed by Klapper [55]. These are summarised in Table 1 and reveal two expected dislocation types: 1A (mixed with an 81 % screw character and growth promoting) and 1B (pure edge character and hence non-growth promoting). The former reflects the projection of the dislocation Burgers vector ½ ⟨1 1 1⟩ onto the growth normal ⟨1 1 0⟩. In this configuration the dislocation is likely to be of mixed character (81 % screw and 19 % edge (see reference [54])). These two configurations can be clearly seen in the X-ray topography study of hexamine by Duckett and Lang [8], are labelled B and A, respectively, in Fig. 13 (b). In this, the lack of co-planarity between the growth direction (n) and the Burgers vector (b) deviates the dislocation line direction (l) away from the facet growth normal. This would be expected to have the effect that these growth-promoting dislocations would, with further growth, tend to move towards the edges of the crystal surfaces as the crystal grows in size, thereby enhancing the opportunities for preferential surface nucleation at the facet edges.

4.4. The role played by crystal chemistry in mediating the growth process

Examination of the intermolecular synthons (see 3.1) reveals that the inclination of synthon A with respect to the {1 1 0} surface would also be expected to promote growth away from the centre of crystal facets. At high supersaturations, synthon A would be likely to promote unstable growth at the under coordinated 3-fold corner sites along the ⟨1 1 1⟩ directions leading, in turn, to the incipient creation of unstable, and potentially dendritic growth. Such a propensity for facet interfacial instability would be consistent with a supersaturation-driven morphological instability. The latter instability possesses a transformation pathway from an initially interfacially-stable planar growth to the formation cavitites and subsequently to unstable dendritic and, following any reduction of supersaturation, back again to the interfacially-stable planar growth. In some way such a morphological instability could be analogous to the well-documented growth of ice crystals as a function of supersaturation and temperature as previously reported [56]. In this

Table 1
Characterisation of growth dislocations for a body centered cubic crystal structure crystallising a {1 1 0} dodecahedral morphology after Roberts (1981).

Type	Growth direction n	Burgers vectors b	Burgers vector magnitude, (Å)	Angle between n and b (°)	Expected character	Screw character, (%)	Step height, (Å)
1A	[1 1 0]	$\frac{1}{2}[111]$	6.00	35.3	Mixed	81	4.89
1B	[1 1 0]	$\frac{1}{2}[\bar{1}11]$	6.00	90.0	Edge	0	0.00

model, 6-member crystal clusters, reflecting this material's hexagonal inherent crystal structure are initially nucleated dendritically but subsequently as supersaturation decreases develop into fully-formed individual crystals.

5. Conclusions

A combination of both x-ray absorption-based computed tomography (also known as x-ray microscopy or XRM) and diffraction contrast tomography (DCT) has revealed the agglomerated crystallisation of hexamine, as prepared from supersaturated ethanolic solutions. This reveals the crystallites within agglomerated particles to be essentially crystallographically aligned. This lattice coherence enables the agglomerates to coalesce, re-seal and overgrow with further growth resulting essentially, in the formation of single crystals of varied internal perfection by this nucleation/growth/ agglomeration crystal growth mechanism. This process traps growth solution through a behaviour that is epitaxial in nature and one which reflects the external morphological symmetry of the initially nucleated 'parent' crystal.

Overall, the work directly supports an agglomeration mechanism in crystal growth, albeit in this case one that has potential impact on the purity of the recrystallized materials. As a result, it highlights the importance of ensuring the stability of the crystal growth interface to ensure crystal quality through careful control of solution supersaturation to restrict the potential for rough interfacial growth. The agglomerative mechanism presented here likely applies to other high symmetry crystal systems, particularly those whose crystal structures involve centred Bravais lattices and where the dominant inter-molecular interactions are angled towards the facet edges. Such structures might also have the potential for edge/corner morphological instabilities in the latter stages of the growth process as crystal size increases. Historical data on ammonium chloride [51] and sodium chloride [57] supports this proposition. Both these materials, like hexamine, belong to cubic high symmetry crystal systems involving structures where their strong inter-molecular synthons lie at oblique angles to the growth surface and where the low energy growth-promoting dislocations are not active at the facet centres.

CRediT authorship contribution statement

Thai T.H. Nguyen: Conceptualization, Methodology, Software, Validation, Formal analysis, Investigation, Data curation, Writing – original draft, Writing – review & editing, Visualization, Project administration. **Parmesh Gajjar:** Conceptualization, Methodology, Software, Validation, Investigation, Data curation, Writing – review & editing, Visualization, Project administration. **Jun Sun:** Software, Investigation, Visualization. **Robert B. Hammond:** Conceptualization, Software, Resources, Supervision, Funding acquisition. **Darragh Murnane:** Conceptualization, Resources, Writing – review & editing, Supervision, Project administration, Funding acquisition. **Benjamin Tordoff:** Resources, Funding acquisition. **Erik Lauridsen:** Resources, Funding acquisition. **Philip J. Withers:** Conceptualization, Resources, Writing – review & editing, Supervision, Funding acquisition. **Kevin J. Roberts:** Conceptualization, Methodology, Resources, Writing – original draft, Writing – review & editing, Supervision, Funding acquisition.

Declaration of Competing Interest

The authors declare the following financial interests/personal relationships which may be considered as potential competing interests: Carl Zeiss Microscopy provided some of the funding for the INFORM2020 project, where one of the authors is employed reports financial support was provided by Carl Zeiss Microscopy GmbH. Some or all of the authors with Xnovo Technology affiliations may have a financial interest in the company. reports a relationship with Xnovo Technology ApS that includes: employment and equity or stocks..

Data availability

Data will be made available on request.

Acknowledgements

The authors wish to acknowledge a highly stimulating workshop on agglomeration as a mechanism for crystal growth organized by Alex Chernov at the 16th International Conference on Crystal Growth (ICCG16) held in Beijing, China in 2010 which stimulated interest on this overall topic and which led, indirectly, to the paper presented here.

This work forms part of the research from the INFORM2020 consortium, which was funded through EPSRC grant EP/N025075/1 "Molecules to manufacture: Processing and Formulation Engineering of Inhalable Nanoaggregates and Micro-particles". We are gratefully acknowledge James Carr and Berzah Yavuzyegit for technical assistance with LabDCT and acknowledge additional funding for this study by Carl Zeiss Microscopy. This work also builds upon research on morphological modelling supported by EPSRC grant EP/I028293/1 "HABIT – Crystal morphology from crystallographic and growth environment factors" and the related Synthonic Engineering programme supported by Pfizer, Boeringer-Ingellheim, Novartis and Syngenta. PG acknowledges support from EP/M010619/1. Beamtime was kindly provided by the Henry Moseley X-ray Imaging Facility (HMXIF), which was established through EPSRC grants EP/F007906/1, EP/I02249X/1 and EP/F028431/1, which is now part of the National Research facility in X-ray CT funded through EPSRC grant EP/T02593X/1. HMXIF is also a part of the Henry Royce Institute for Advanced Materials which was established through EPSRC grants EP/R00661X/1, EP/P025498/1 and EP/P025021/1.

References

[1] A. Bulterov, Hexamethylenetetramine, Justus Liebigs Ann. Chem. 11 (1859) 250.
[2] R.G. Dickinson, A.L. Raymond, The crystal structure of hexamethylene-tetramine, J. Am. Chem. Soc. 45 (1) (1923) 22–29.
[3] R. Brill, H. Grimm, C. Hermann, C. Peters, Anwendung der röntgenographischen Fourieranalyse auf Fragen der chemischen Bindung, Ann. Phys. 426 (5) (1939) 393–445.
[4] R.W.G. Wyckoff, R.B. Corey, Spectrometric Measurements on Hexamethylene Tetramine and Urea, Zeitschrift für Kristallographie - Crystalline Materials 89 (1–6) (1934) 462–468.
[5] N. Blažzević, D. Kolbah, B. Belin, V. Šunjić, F. Kajfež, Hexamethylenetetramine, a versatile reagent in organic synthesis, Synthesis 1979 (03) (1979) 161–176.
[6] A.S. Myerson, S.E. Decker, W. Fan, Solvent selection and batch crystallization, Ind. Eng. Chem. Process Des. Dev. 25 (4) (1986) 925–929.
[7] C. Forno, The growth of large crystals of hexamine from solution, J. Cryst. Growth 21 (1) (1974) 61–64.
[8] R.A. Duckett, A.R. Lang, The growth of nearly perfect hexamethylenetetramine crystals from solution, J. Cryst. Growth 18 (2) (1973) 135–142.
[9] G.E. Gottlieb, The Controlled Sublimation Technique and Its Utilization for the Crystal Growth of Hexamine, J. Electrochem. Soc. 112 (9) (1965) 903.
[10] A. Alamdari, F. Tabkhi, Kinetics of hexamine crystallization in industrial scale, Chem. Eng. Process. 43 (7) (2004) 803–810.
[11] J. Bourne, R. Davey, The growth of hexamethylene tetramine crystals from ethanolic solutions, J. Cryst. Growth 34 (2) (1976) 230–238.
[12] J. Bourne, R. Davey, H. Gros, K. Hungerbühler, The rotating disc configuration in the measurement of crystal growth kinetics from solution, J. Cryst. Growth 34 (2) (1976) 221–229.
[13] R. Davey, A. Rütti, Agglomeration in the crystallisation of hexamethylene tetramine from aqueous solution, J. Cryst. Growth 32 (2) (1976) 221–226.
[14] K.G. Denbigh, E. White, Studies on liquid inclusions in crystals, Chem. Eng. Sci. 21 (9) (1966) 739–753.
[15] E.T. White, The formation and drying out of liquid inclusions in crystals. PhD thesis. 1964, Imperial College London, UK.
[16] J.W. Gibbs, On the equilibrium of heterogeneous substances, Am. J. Sci. Arts (1820-1879) 16 (96) (1878) 441–458.
[17] G. Wulff, XXV. Zur frage der geschwindigkeit des wachsthums und der auflösung der krystallflächen, Zeitschrift für Kristallographie-Crystalline Materials 34 (1–6) (1901) 449–530.
[18] S. O'hara, L. Tarshis, W. Tiller, J. Hunt, Discussion of interface stability of large facets on solution grown crystals, J. Cryst. Growth 3-4 (1968) 555–561.
[19] J.C. Brice, T.M. Bruton, The stability of facets on growing crystals, J. Cryst. Growth 26 (1) (1974) 59–60.
[20] C.C. Sun, Materials Science Tetrahedron—A Useful Tool for Pharmaceutical Research and Development, J. Pharm. Sci. 98 (5) (2009) 1671–1687.

[21] B.Y. Shekunov, P. York, Crystallization processes in pharmaceutical technology and drug delivery design, J. Cryst. Growth 211 (1–4) (2000) 122–136.
[22] S. Datta, D.J. Grant, Crystal structures of drugs: advances in determination, prediction and engineering, Nat. Rev. Drug Discov. 3 (1) (2004) 42–57.
[23] N. Feeder, E. Pidcock, A.M. Reilly, G. Sadiq, C.L. Doherty, K.R. Back, P. Meenan, R. Docherty, The integration of solid-form informatics into solid-form selection, J. Pharm. Pharmacol. 67 (6) (2015) 857–868.
[24] P. Gajjar, T.T.H. Nguyen, J. Sun, I.D. Styliari, H. Bale, S.A. McDonald, T.L. Burnett, B. Tordoff, E. Lauridsen, R.B. Hammond, D. Murnane, P.J. Withers, K.J. Roberts, Crystallographic tomography and molecular modelling of structured organic polycrystalline powders, CrstEngComm 23 (13) (2021) 2520–2531.
[25] G.R. Desiraju, Supramolecular synthons in crystal engineering—a new organic synthesis, Angew. Chem. Int. Ed. Eng. 34 (21) (1995) 2311–2327.
[26] T.T.H. Nguyen, R.B. Hammond, I.D. Styliari, D. Murnane, K.J. Roberts, A digital workflow from crystallographic structure to single crystal particle attributes for predicting the formulation properties of terbutaline sulfate, CrstEngComm 22 (19) (2020) 3347–3360.
[27] R. Docherty, G. Clydesdale, K.J. Roberts, P. Bennema, Application of Bravais-Friedel-Donnay-Harker, attachment energy and Ising models to predicting and understanding the morphology of molecular crystals, J. Phys. D Appl. Phys. 24 (2) (1991) 89–99.
[28] I. Rosbottom, K. Roberts, R. Docherty, The solid state, surface and morphological properties of p-aminobenzoic acid in terms of the strength and directionality of its intermolecular synthons, CrstEngComm 17 (30) (2015) 5768–5788.
[29] T.T. Nguyen, I. Rosbottom, I. Marziano, R.B. Hammond, K.J. Roberts, Crystal morphology and interfacial stability of RS-Ibuprofen in relation to its molecular and synthonic structure, Cryst. Growth Des. 17 (6) (2017) 3088–3099.
[30] T.D. Turner, L.E. Hatcher, C.C. Wilson, K.J. Roberts, Habit Modification of the API Lovastatin through a Predictive Solvent Selection Approach, J. Pharm. Sci. 108 (5) (2019) 1779–1787.
[31] G. Clydesdale, R.B. Hammond, K.J. Roberts, Molecular Modeling of Bulk Impurity Segregation and Impurity-Mediated Crystal Habit Modification of Naphthalene and Phenanthrene in the Presence of Heteroimpurity Species, J. Phys. Chem. B 107 (20) (2003) 4826–4833.
[32] G. Clydesdale, G.B. Thomson, E.M. Walker, K.J. Roberts, P. Meenan, R. Docherty, A Molecular Modeling Study of the Crystal Morphology of Adipic Acid and Its Habit Modification by Homologous Impurities, Cryst. Growth Des. 5 (6) (2005) 2154–2163.
[33] R.B. Hammond, V. Ramachandran, K.J. Roberts, Molecular modelling of the incorporation of habit modifying additives: α-glycine in the presence of l-alanine, CrstEngComm 13 (15) (2011) 4935–4944.
[34] K.J. Roberts, R.B. Hammond, V. Ramachandran, R. Docherty, Synthonic engineering: from molecular and crystallographic structure to the rational design of pharmaceutical solid dosage forms, chapter 7, in Y.A. Abramov (Ed.), Computational Pharmaceutical Solid State Chemistry, Wiley, 2016, pp. 175–210.
[35] J. Pickering, R.B. Hammond, V. Ramachandran, M. Soufian, K.J. Roberts, *Synthonic engineering modelling tools for product and process design*, in: K. Roberts, R. Docherty, R. Tamura (Eds.), Engineering Crystallography: From Molecule to Crystal to Functional Form, Springer Science + Business Media, 2017, pp. 155–176.
[36] M. Bunker, M. Davies, C. Roberts, Towards screening of inhalation formulations: measuring interactions with atomic force microscopy, Expert Opin. Drug Deliv. 2 (4) (2005) 613–624.
[37] S.P. Kampermann, T.M. Sabine, B.M. Craven, R.K. McMullan, Hexamethylenetetramine: extinction and thermal vibrations from neutron diffraction at six temperatures, Acta Crystallographica Section A: Foundations of Crystallography. 51 (4) (1995) 489–497.
[38] F. Bachmann, H. Bale, N. Gueninchault, C. Holzner, E.M. Lauridsen, 3D grain reconstruction from laboratory diffraction contrast tomography, J. Appl. Cryst. 52 (3) (2019) 643–651.
[39] L.A. Feldkamp, L.C. Davis, J.W. Kress, Practical cone-beam algorithm, J. Opt. Soc. Am. A 1 (6) (1984) 612–619.
[40] G. Clydesdale, K. Roberts, R. Docherty, Computational studies of the morphology of molecular crystals through solid-state intermolecular force calculations using the atom-atom method, in: Controlled Particle, Droplet and Bubble Formation, Butterworth-Heinemann, 1994, pp. 95–135.
[41] S.L. Mayo, B.D. Olafson, W.A. Goddard, DREIDING: a generic force field for molecular simulations, J. Phys. Chem. 94 (26) (1990) 8897–8909.
[42] G. Clydesdale, K. Roberts, R. Docherty, HABIT95—a program for predicting the morphology of molecular crystals as a function of the growth environment, J. Cryst. Growth 166 (1–4) (1996) 78–83.
[43] J.D.H. Donnay, D. Harker, A new law of crystal morphology extending the law of Bravais, Am. Mineral.: J. Earth Planet. Mater. 22 (5) (1937) 446–467.
[44] G. Friedel, Etudes sur la loi de Bravais, Bull. Minér. 30 (9) (1907) 326–455.
[45] A. Bravais, Etudes Cristallographiques. Gauthier-Villars, Paris, 1866.
[46] P. Hartman, P. Bennema, The attachment energy as a habit controlling factor: I. Theoretical considerations, J. Cryst. Growth 49 (1) (1980) 145–156.
[47] K.G. Denbigh, E.T. White, Regular Inclusion Pattern in Crystals, Nature 199 (4895) (1963) 799–800.
[48] M.H.R.J. Plusjé, W.J. Dunning, W.K. Burton, N. Cabrera, R.F. Strickland-Constable, S. Fordham, F.C. Frank, W.E. Garner, K.G. Denbigh, W.A. Wooster, D.R. Hale, A. Juliard, A.E. Robinson, L.J. Griffin, I.N. Stranski, C.W. Bunn, Y. Haven, E. O. Hall, H.K. Hardy, H.E.E. Powers, A.F. Wells, A.R. Ubbelohde, J. Lennard-Jones, General discussion, Discuss. Faraday Soc. 5 (1949) 183–197.
[49] W. Berg, Crystal growth from solutions, Proc. Roy. Soc. Lond. Series A-Math. Phys. Sci., 164 (916) (1938), 79-95.
[50] C. Bunn, Crystal growth from solution. II. Concentration gradients and the rates of growth of crystals, Discuss. Faraday Soc. 5 (1949) 132–144.
[51] C.W. Bunn, Crystals: Their Role in Nature and in Science, Academic Press, New York and London, 1964.
[52] J.W. Mullin, Crystallization, fourth ed., Butterworth-Heinemann, Oxford, 2001.
[53] W. Burton, N. Cabrera, F.C. Frank, The growth of crystals and the equilibrium structure of their surfaces, Philosophical Transactions of the Royal Society of London. Series A, Mathematical and Physical Sciences 243 (1951) 299–358.
[54] K.J. Roberts, Dislocations in $Y_3Al_5O_{12}$, J. Mater. Sci. 16 (9) (1981) 2517–2520.
[55] H. Klapper, Defects in non-metal crystals, in: B.K. Tanner, D.K. Bowen, (Eds.), Characterization of Crystal Growth Defects by X-Ray Methods, Nato Advanced Study Institutes Series, vol 63, Springer, Boston, MA, 1980, pp.133-160.
[56] K.G. Libbrecht, Physical dynamics of ice crystal growth, Annu. Rev. Mat. Res. 47 (2017) 271–295.
[57] J.D. Birchall, Private Communication, 1964, cited in the reference [14].